

Defect-mediated melting of Xe adsorbed on the Si(100)- 2×1 surface: A molecular-dynamics study

Rafael Ramírez and Luis Utrera

Instituto de Ciencia de Materiales, Consejo Superior de Investigaciones Científicas, Serrano 115 Duplicado, 28006 Madrid, Spain

(Received 30 July 1992)

The melting of a Xe adlayer over the Si(100)- 2×1 surface at a coverage $\Theta=0.85$ has been studied by molecular-dynamics simulation. The substrate is characterized by large surface corrugation and anisotropy, i.e., different corrugation along the x and y axes. The melting of the adlayer is strongly influenced by the anisotropy of the substrate. Static and dynamic properties of the adatoms have been investigated for temperatures between 80 and 220 K. The melting transition proceeds in two steps at temperatures $T_I=135$ K and $T_{II}=174$ K. Both transitions can be described by the Kosterlitz-Thouless theory of dislocation-mediated melting. The two-dimensional (2D) solid is commensurate with the substrate along the x direction, but it is incommensurate along the y axis, where the substrate corrugation is lower. The intermediate phase is described as a 1D lattice liquid in which the adatoms are confined along the x axis by the highest-energy barriers of the surface potential, and display liquidlike behavior along the perpendicular direction. The high-temperature phase corresponds to a 2D lattice liquid.

I. INTRODUCTION

The melting of physisorbed overlayers on solid substrates has attracted considerable theoretical and experimental interest in the past decade.^{1,2} The Kosterlitz-Thouless theory,³ which was further developed by Nelson and Halperin⁴ and Young,⁵ suggests that two-dimensional (2D) solids might melt by unbinding of pairs of crystal defects. The quasi-long-range positional order of the 2D solid would be destroyed by the unbinding of dislocation pairs, leading to a hexatic phase. At higher temperature a second transition due to the unbinding of disclination pairs would destroy the long-range orientational order of the hexatic phase, driving the system to an isotropic liquid. Both transitions are predicted by the theory to be continuous.

Experimental evidence for continuous melting has been reported for high-coverage incommensurate overlayers of Xe (Ref. 6) and Kr (Ref. 7) on graphite, as well as for some molecules, such as physisorbed ethylene⁸ and intercalated nitric acid⁹ in graphite. However, at submonolayer coverage the melting of Xe,¹⁰ Ne,¹¹ CH₄,¹² and O₂ (Ref. 13) on graphite has been found to be first order. The diversity of melting characteristic exhibited by physisorbed atoms or molecules on graphite is then quite surprising. A variety of factors can influence the 2D melting process, e.g., the corrugation and anisotropy of the substrate potential, the motion of atoms perpendicular to the surface, and the exchange of atoms between the gas and the adlayer. These factors are difficult to handle on the basis of analytical models for 2D melting. In this context, computer simulation experiments appear as a valuable tool to overcome this difficulty.

Computer simulations based on the Monte Carlo (MC) method have been performed in order to study the effect of the substrate potential on several properties (internal energy, order parameters) of commensurate physisorbed overlayers.¹⁴ The simulations reported by Abraham² for 2D Lennard-Jones systems led to the conclusion that the

2D melting transition should be first order, in contradiction with the renormalization-group arguments of Halperin and Nelson. A molecular-dynamics (MD) study of ethylene on graphite¹⁵ found a continuous melting transition in agreement with experimental results.⁸ A critical review of simulation results concerning the 2D melting transition is given in Ref. 1.

Although most studies concerning 2D melting have been performed on graphite, it is important to extend these investigations to substrates with different characteristics. The basal plane of graphite is a prototype of an isotropic surface with low corrugation. However, the Si(100)- 2×1 surface displays large corrugation as well as anisotropy, i.e., different surface corrugation along the x and y directions, which influence the physical properties (structure, diffusion, melting) of adsorbed atoms. The Si(100) surface has been the subject of a large number of studies mainly centered on the surface reconstruction,¹⁶ electronic properties,¹⁷ as well as some dynamical processes (self-diffusion of Si atoms).¹⁸ Adsorption of alkali-metal atoms on this surface has been widely investigated as a prototype of a metal-semiconductor interphase.¹⁹ We have previously reported MD simulations devoted to the commensurate-incommensurate transition of physisorbed Xe atoms as a function of coverage.²⁰ The jump mechanism responsible for Xe diffusion on this surface was also investigated by the same technique.²¹

In the present contribution we have studied the melting of a Xe overlayer at coverage $\Theta=0.85$ on the Si(100)- 2×1 surface by MD simulation. The static and dynamic properties of the adlayer at temperatures in the range 80–220 K reveal that the melting occurs in two steps as a consequence of the anisotropy induced by the solid substrate. The first transition ($T_I=135$ K) is driven by the unbinding of dislocation pairs whose Burger's vectors are oriented along the y direction. Due to the substrate anisotropy topological defects are preferentially formed along the y axis. At a higher temperature ($T_{II}=174$ K), a second transition drives the system to a

2D lattice liquid. This transition is due to the unbinding of dislocation pairs with a finite component along the x axis. The intermediate phase over the anisotropic Si surface has been described as a 1D lattice liquid.

II. COMPUTATIONAL MODEL

The structural model of Holland, Duke, and Paton²² for the Si(100)- 2×1 surface has been employed in the simulation. The lattice parameters of the 2D rectangular unit cell are $a_c = 7.68 \text{ \AA}$ and $b_c = 3.84 \text{ \AA}$. The subindex c will be used in this paper as a symbol for commensurate periodicity. A schematic representation of the surface is given in Fig. 1. The topmost surface atoms form Si dimers arranged in rows along the y direction. Between two contiguous Si dimer rows there appear surface grooves which extend also parallel to the lattice vector \mathbf{b}_c . The 2D unit cell of the substrate includes two Si atoms. Local minima for the Xe-Si surface potential are found over surface grooves (site G) and over Si dimer rows (site D), respectively.

The Xe-Xe and Xe-Si interactions have been modeled by Lennard-Jones 12:6 potentials with the following parameters: $\epsilon_{\text{Xe-Xe}} = 1.9 \text{ kJ/mol}$, $\sigma_{\text{Xe-Xe}} = 4.06 \text{ \AA}$, $\epsilon_{\text{Xe-Si}} = 1.6 \text{ kJ/mol}$, $\sigma_{\text{Xe-Si}} = 3.9 \text{ \AA}$ (see Ref. 21 for further details on the interatomic potentials). This model implies that induction effects are not explicitly included. However, they are expected to be small for a nonionic substrate. The Si atoms were not allowed to move during the MD simulation. This approximation is justified by the low-energy electron diffraction (LEED) data of Ref. 23, which indicate that the structure of Si(111)- 7×7 is not appreciably modified by Xe adsorption. Moreover, a microscopic force model estimates that the adsorbed Xe atoms would compress the Si-Si bond by only $3.5\times 10^{-3} \text{ \AA}$.²³ One expects that a small substrate relaxation of the same order of magnitude will appear in the case of the Si(100)- 2×1 surface.

The anisotropy of the substrate potential can be inferred from Fig. 2. The interatomic Xe-substrate potential affecting an isolated Xe atom is displayed along the translation vectors \mathbf{a}_c and \mathbf{b}_c . The curves are labeled as $V(x,0)$ and $V(0,y)$, respectively. At each surface position the z coordinate of the Xe atom was varied in order to obtain the minimum potential. The surface corruga-

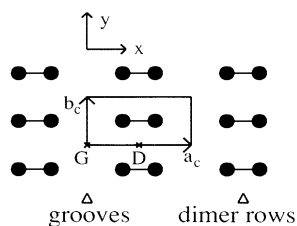


FIG. 1. Schematic representation of the topmost Si layer of the Si(100)- 2×1 surface. The rectangular unit cell is shown. The local minima for the Xe-Si potential are found at sites G and D . The Si surface consists of parallel rows of Si dimers with surface grooves between them.

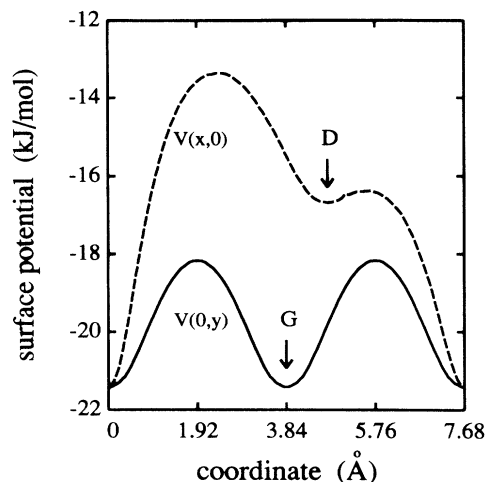


FIG. 2. Surface potential along the translation vectors \mathbf{a}_c and \mathbf{b}_c of the Si(100)- 2×1 surface. The potential curves are labeled as $V(x,0)$ and $V(0,y)$, respectively. The interval displayed for the horizontal axis corresponds to the cell parameter $a_c = 2b_c = 7.68 \text{ \AA}$.

tion is more pronounced along the x direction, where the energy barriers are roughly two times larger than those encountered along the y direction. The asymmetry of the $V(x,0)$ curve is due to the asymmetric Si dimer model employed in the simulation.²² The binding energies associated to the local minima on sites G and D are 21.4 and 16.7 kJ/mol. Experimental values reported from the thermal desorption spectra of Xe/Si(100)- 2×1 were 19.5 and 16.9 kJ/mol.²⁴ The z coordinate corresponding to the local minima on sites G and D are 2.6 and 3.3 \AA . This difference in the z coordinate is a consequence of the surface corrugation. The topmost Si atoms are located at $z=0$.

The simulation cell employed in the calculations corresponds to a 10×20 superlattice with dimensions $76.8\times 76.8 \text{ \AA}^2$. Periodic boundary conditions were applied during the simulation. At each temperature large equilibration runs up to 400 ps were performed starting from an initial configuration with the adatoms located at a height of about 5 \AA above the surface. After equilibration, averaged properties of the system were calculated in the microcanonical ensemble by sampling on trajectories up to 400 ps. The time step employed in the Verlet algorithm for the numerical integration of the motion equations amounts to 10^{-14} s . The total energy fluctuates under these conditions by less than 0.01%.

The density of Si atoms on the Si(100)- 2×1 surface is $n_{\text{Si}} = 6.78\times 10^{14} \text{ atoms/cm}^2$ (i.e., two Si atoms per substrate unit cell, see Fig. 1). The density of a full monolayer of Xe atoms is, after the MD simulation, $n_{\text{Xe}} = 0.85n_{\text{Si}}$ (i.e., 1.7 Xe atoms per unit cell). The last value has been taken for the definition of coverage $\Theta = 1$. The present simulation has been performed for Xe coverage $\Theta = 0.85$ (i.e., 1.45 atoms per unit cell). At this coverage and at low temperature the adlayer structure is "out of register" (incommensurate) with the substrate

along the y direction but it is commensurate along the x one. This effect is due to the anisotropy of the surface potential. The adatoms build a rectangular centered lattice with nearly hexagonal symmetry. The corresponding lattice parameters are $a_c = 7.68 \text{ \AA}$ and $b_i = 4.8 \text{ \AA}$.

Several ensemble averaged properties have been calculated in the temperature range 80–220 K in order to characterize the 2D melting transition. The static structure factor $S(\mathbf{k})$ of the adatoms is defined as

$$S(\mathbf{k}) = \frac{1}{N^2} \left\langle \left| \sum_{p=1}^N \exp(i2\pi\mathbf{k}\cdot\mathbf{r}_p) \right|^2 \right\rangle, \quad (1)$$

where N is the number of Xe atoms in the simulation cell, \mathbf{r}_p is the projection of the position vector of adatom p on the xy plane, and \mathbf{k} is a vector in the 2D reciprocal space. The angle brackets $\langle \rangle$ represent the average value over the whole trajectory. $S(\mathbf{k})$ has been calculated for \mathbf{k} vectors corresponding to the reciprocal lattice of the supercell employed in the simulation. These k points build a square mesh where the distance between contiguous k points amounts to 0.013 \AA^{-1} .

The orientational order parameter p_6 of the adatoms is defined as

$$p_6 = \frac{1}{6N} \left\langle \left| \sum_{p=1}^N \sum_{q=1}^{n_i} \exp(i6\alpha_{pq}) \right| \right\rangle, \quad (2)$$

where the sum on q runs over the n_i nearest neighbors of atom p and α_{pq} is the angle between the interatomic vector \mathbf{r}_{pq} and the y axis.

The pair-distribution function is given by

$$g(\mathbf{r}) = \frac{S}{N^2} \left\langle \sum_{p=1}^N \sum_{q \neq p}^N \delta(\mathbf{r} - \mathbf{r}_{pq}) \right\rangle, \quad (3)$$

S is the area of the simulation cell and δ is the Kronecker delta function. Surface self-diffusion coefficients have been calculated by means of the Einstein formula

$$D_s = \lim_{t \rightarrow \infty} \frac{\langle x^2(t) \rangle + \langle y^2(t) \rangle}{4t}, \quad (4)$$

where t is the time and $\langle x^2(t) \rangle$ and $\langle y^2(t) \rangle$ denote the mean-square displacement (MSD) of a particle in the x and y directions, respectively. The MSD's are calculated from the trajectories as a double average over particles and noncorrelated time origins:

$$\langle x^2(t) \rangle = \frac{1}{N_\tau N} \sum_{\tau=1}^{N_\tau} \sum_{p=1}^N [x_p(\tau+t) - x_p(\tau)]^2. \quad (5)$$

In this formula $x_p(t)$ corresponds to the x component of the position vector of particle p at time t . N_τ is the number of different time origins used in the average. A similar expression holds for the y coordinate.

III. POINT AND EXTENDED DEFECTS ON THE 2D SOLID

Visual inspection of the adatom configurations generated during the MD simulation allows us to identify the nature of extended and point defects in the 2D solid. In

Fig. 3 we show a projection on the xy plane of an instantaneous configuration of the adlayer atoms at temperature $T=80 \text{ K}$. Black circles represent Xe atoms adsorbed over the surface grooves, gray circles represent adatoms over Si dimer rows, and open squares symbolize atom vacancies. Note that the adatoms are adsorbed on a centered rectangular lattice with nearly hexagonal symmetry. As the representation corresponds to an instantaneous configuration, adatom vibrations at the studied temperature appear as distortions of the perfect adatom lattice. The atom vacancies are found either isolated or in pairs over the Si dimer rows, which are the adsorption positions of lower binding energy. It is remarkable that in spite of the finite size of the simulation cell, extended defects are also found in the adlayer structure. Dislocations are indicated by arrows pointing along the direction of the corresponding Burger's vector. The arrows are placed near fivefold coordinated adatoms, which represent terminal points for atomic rows forming an angle to the horizontal axis of about $\pm 30^\circ$. These atoms are displayed as open circles in Fig. 3. The dislocations appear in pairs as expected for a 2D solid. The elementary Burger's vectors corresponding to a rectangular centered lattice are shown in Fig. 4. By symmetry the six vectors are divided into two different groups labeled as I and II. It is important to note that the Burger's vectors of the dislocation pairs found at $T=80 \text{ K}$ are always oriented along the y axis (type-I dislocations). This preferential behavior is a consequence of the anisotropy of the substrate potential. Dislocations whose Burger's vectors have an x component different from zero (type-II dislocations) have higher energy and they are not found at low

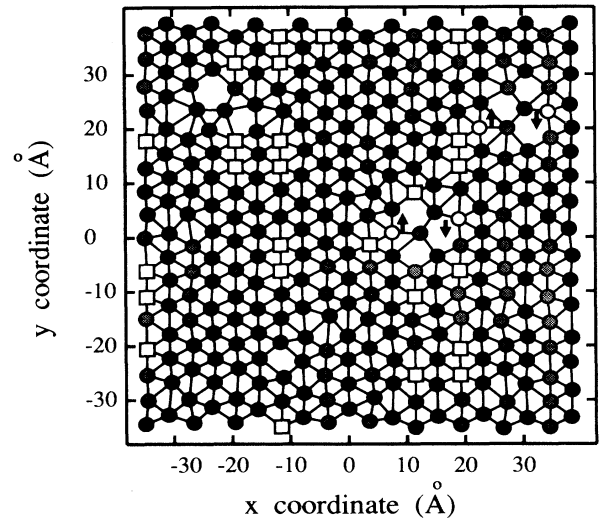


FIG. 3. Structure corresponding to an instantaneous adlayer configuration at $T=80 \text{ K}$. The xy projection covers the whole simulation cell. Black and gray circles distinguish adatoms adsorbed over surface grooves and Si dimer rows, respectively. Open squares represent atom vacancies. The arrows near the fivefold coordinated atoms displayed as open circles are parallel to the Burger's vector of the dislocations. The dislocations appear in pairs in the 2D solid.

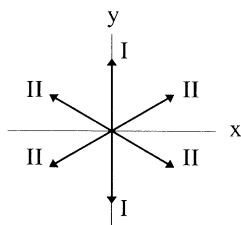


FIG. 4. Schematic representation of the Burger's vector associated to type-I and type-II dislocations. Formation of type-I dislocations is favored with respect to type II due to the anisotropy of the surface potential.

temperature. Another interesting fact is the different role of atom vacancies associated to the two adsorption sites on this surface. Vacancies corresponding to the less stable adsorption site over the Si dimer rows appear as point defects. However, vacancies associated to the most stable adsorption site (surface grooves) take part of an extended defect (dislocation pair).

Disclinations may also play an important role in the 2D melting process. At low temperatures it is expected to find disclination quartets in the 2D solid. A typical example obtained from the simulation at $T=80$ K is shown in Fig. 5. The disclination quartets are created from the perfect adatom lattice by small displacements of four six-fold coordinated atoms to give two fivefold and two sevenfold coordinated adatoms.

IV. MELTING TRANSITION

The internal energy and reduced pressure ($P\sigma_{\text{Xe-Xe}}^2/\epsilon_{\text{Xe-Xe}}$) of the Xe adatoms are displayed in Fig. 6 for 17 temperatures in the interval $T=80$ –220 K. We observe changes in the slope of the curves at $T_I=135$ K and $T_{II}=174$ K, which are a first indication of a two-step process in the melting of the adlayer. Below the temperature T_I all Xe atoms in the simulation cell are adsorbed on the first adlayer. At temperature $T_I=135$ K the promotion of adatoms to the second adlayer begins. Atomic distribution functions calculated along the z direction al-

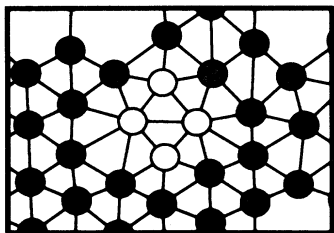


FIG. 5. A disclination quartet can be described as a set of four atoms, two of them having five neighbors and the other two having seven neighbors. These four atoms are displayed as open circles. Black and gray circles have the same meaning as in Fig. 3. The example corresponds to a configuration obtained at $T=80$ K.

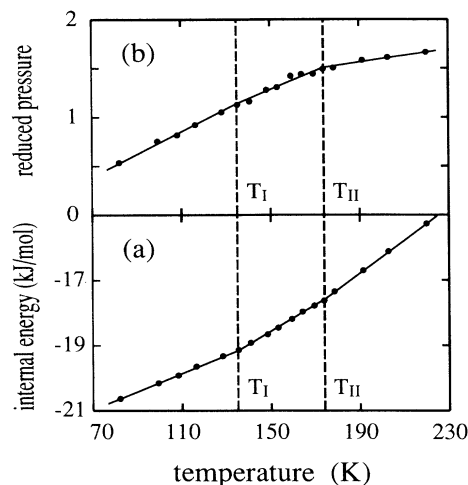


FIG. 6. (a) Internal energy and (b) reduced pressure $P\sigma_{\text{Xe-Xe}}^2/\epsilon_{\text{Xe-Xe}}$ of the Xe adlayer as a function of the temperature. The changes in the slope of the curves at temperatures $T_I=135$ K and $T_{II}=174$ K are related to the melting of the adlayer.

lowed us to derive a coordinate $z=5$ Å as a criterion to distinguish between the first and the second adlayer. The variation of the density of the first adlayer as a function of temperature is displayed in Fig. 7. The curve suggests the existence of three different phases separated by the temperatures T_I and T_{II} .

In the following, several structural and dynamic properties of the adatoms are analyzed as a function of the temperature. In particular, we are interested in finding if the transitions at temperatures T_I and T_{II} are related to the unbinding of topological defects, as predicted by the Kosterlitz-Thouless theory of 2D melting. The structure

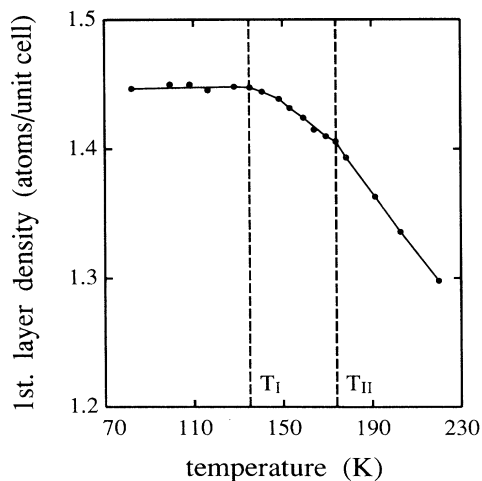


FIG. 7. Temperature dependence of the density of adatoms in the first adlayer. The density is given as number of atoms per unit cell of the solid substrate. Vertical lines indicate the temperatures where transitions are found.

factor $S(\mathbf{k})$ of the adatoms as a function of temperature for the direction $k_y=0$ in reciprocal space is shown in Fig. 8. The peaks in the $S(\mathbf{k})$ curves appear at reciprocal points associated to a periodicity $a_c=7.68 \text{ \AA}$ in real space. These points are labeled as $(h,0)_c$ in the figure. The long-range order imposed by the corrugated substrate does not disappear as a function of the temperature. Therefore along the x axis the adlayer structure remains commensurate with the substrate in the whole studied temperature range.

The temperature dependence of $S(\mathbf{k})$ for the direction $k_x=0$ is shown in Fig. 9 for the interval $0.3 \leq k_y \leq 0.6 \text{ \AA}^{-1}$. In this region we find $(0,2)_c$ and $(0,2)_i$ peaks. The $(0,2)_c$ peak corresponds to the commensurate periodicity in real space given by $b_c=3.84 \text{ \AA}$, while the $(0,2)_i$ peak is associated to the periodicity $b_i=4.8 \text{ \AA}$, characteristic of the incommensurate solid. The $(0,1)_i$ peak at $k_y=0.208 \text{ \AA}^{-1}$ corresponds to a systematic extinction in the rectangular centered lattice of the 2D solid. We observe that below the temperature $T_I=135 \text{ K}$ (i.e., the curves corresponding to the four lowest temperatures in Fig. 9) the $(0,2)_i$ peak is higher than the $(0,2)_c$ peak. Moreover, above the temperature T_I the $(0,2)_i$ peak disappears, giving rise to a diffuse scattering profile. Two structural consequences can be derived from this behavior. First, the long-range order associated to the b_i periodicity is lost at temperatures above $T_I=135 \text{ K}$. A second effect is that the positional correlation between parallel rows of atoms along the y direction is also lost at temperatures $T > T_I$. In Sec. III it was shown that the most relevant topological defects associated to the 2D solid were dislocation pairs of type I. The above-mentioned structural effects can be understood by the unbinding of these dislocation pairs at temperature $T_I=135 \text{ K}$. The resulting phase, where the $b_i=4.8 \text{ \AA}$ periodicity is lost because of positional disorder along the y direction, will be referred to as a 1D lattice liquid (see below).

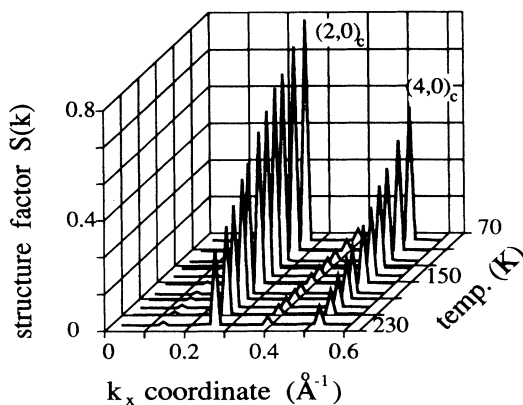


FIG. 8. Temperature dependence of the structure factor $S(\mathbf{k})$ of the adatoms along the direction $k_y=0$ in reciprocal space. The $S(\mathbf{k})$ peaks appear at k_x coordinates related to the periodicity $a_c=7.68 \text{ \AA}$ in real space. The $S(\mathbf{k})$ values at $k_x=0$ are 1 and they are not shown in the figure.

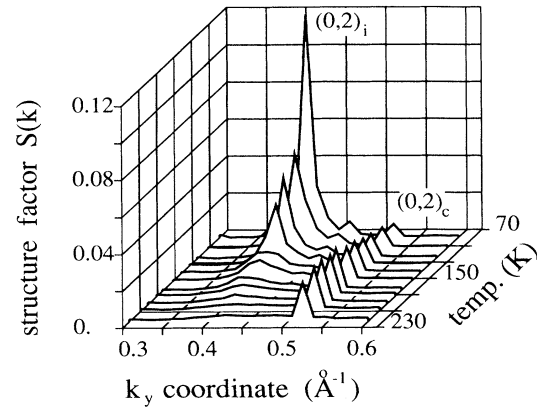


FIG. 9. Structure factor $S(\mathbf{k})$ of the adatoms along $k_x=0$ as a function of the temperature. The subindex i (c) of the $S(\mathbf{k})$ peak refers to the b_i (b_c) periodicity along the y axis in real space. The $(0,1)_i$ peak corresponds to a systematic extinction in the 2D solid and it is not shown in the figure.

The $S(\mathbf{k})$ values corresponding to the $(0,2)_c$ point in reciprocal space as well as the orientational order parameter p_6 of the adatoms are shown in Fig. 10 as a function of the temperature. Both curves differ by a vertical shift. This fact indicates that both positional and orientational order parameters are strongly correlated in the studied temperature range. Above the temperature $T_{II}=174 \text{ K}$ we observe a distinct temperature dependence of the $S(\mathbf{k})$ curve, which we associate to a transition to a 2D lattice liquid due to the unbinding of type-II dislocation pairs (i.e., dislocations whose Burger's vector has a finite x component). At temperatures above T_{II} the $S(\mathbf{k})$ values follow a $(V_{2,0}/k_B T)^2$ dependence, which has been represented by a solid line. This behavior is predicted by

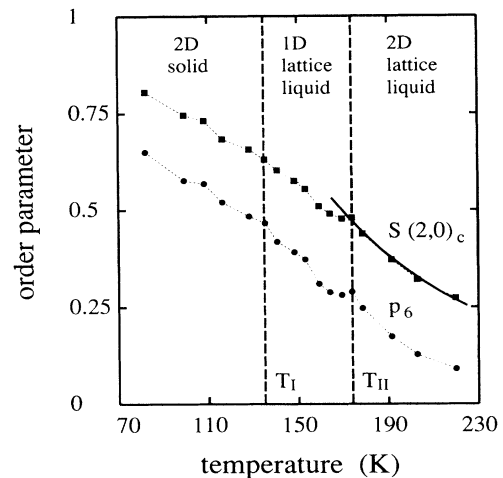


FIG. 10. Structure factor for the $(2,0)_c$ reciprocal point and orientational order parameter p_6 of the adatoms as a function of the temperature. The solid line indicates the result of the linear theory by Reiter and Moss (Ref. 25).

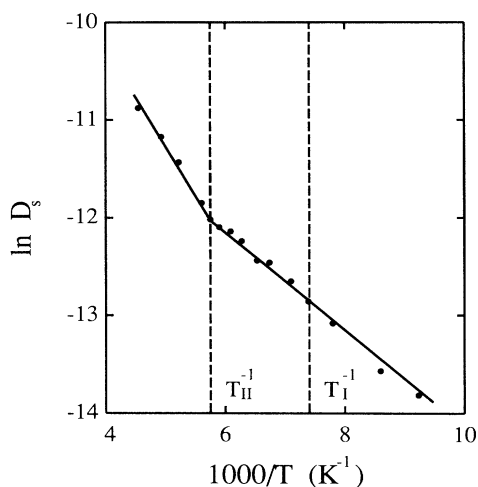


FIG. 11. Arrhenius plot of the self-diffusion coefficient D_s of the Xe atoms adsorbed in the first adlayer for temperatures between 80 and 220 K. The slope of the curve changes at the temperature $T_{II}=174$ K.

the Reiter-Moss theory of the scattering properties of a 2D lattice liquid.²⁵ The parameter $V_{2,0}$ is the (2,0) Fourier component of the substrate potential. The solid line in the figure corresponds to a value $V_{2,0}=1.06$ kJ/mol. A derivation of the $V_{2,0}$ parameter from the applied potential model is difficult because of the z dependence of both the surface potential and the trajectories actually followed by the adatoms. We can estimate this parameter by considering the potential surface $V(x,y)$ calculated by minimization of the surface potential at each (x,y) position with respect to the z coordinate. The (2,0) Fourier coefficient of this potential surface is 0.75 kJ/mol, i.e., smaller than the parameter $V_{2,0}=1.06$ kJ/mol derived from the $S(\mathbf{k})$ values. This difference may be due to the uncertainty introduced by the z dependence of the actual surface potential or to limitations of the linear approach in the Reiter-Moss theory.²⁵

We turn now to study the influence of the transitions at temperatures T_I and T_{II} on the dynamic properties of the adatoms. The temperature dependence of the self-diffusion coefficient D_s of the Xe atoms of the first adlayer was derived by means of the Einstein relation [see Eq. (4)]. The one-dimensional diffusion coefficients D_x and D_y were calculated as well. In the analysis of the

adatom trajectories we excluded those Xe atoms promoted to the second adlayer. In fact, the MSD's associated to these atoms are not proportional to the time t ; instead they show a time dependence close to t^2 . This means that the adatoms on the second adlayer move in an inertial regime rather than in a diffusional one. The Arrhenius plot of the self-diffusion coefficient D_s is presented in Fig. 11. Two different diffusion regimes are distinguished at temperatures above and below $T_{II}=174$ K. The corresponding preexponential factors (D_0) and activation energies (E_a) are summarized in Table I together with the values associated to one-dimensional self-diffusion coefficients D_x and D_y . It is interesting to note that the activation energies E_a for adatom diffusion along the x direction (i.e., 8.3 and 5.0 kJ/mol in the high- and low-temperature regimes, respectively) correspond closely to the static energy barriers displayed in Fig. 2 (i.e., 8.1 and 5.0 kJ/mol). The E_a values for adatom diffusion along the y direction (i.e., 7.2 and 4.2 kJ/mol) are about 15% lower than the activation energies along the x direction, i.e., much larger than the static barrier of 3.2 kJ/mol. Diffusive paths of adatoms involving jumps along the y direction (lower surface corrugation) are not possible without jumps in the perpendicular direction. This behavior is not surprising due to the relative high coverage considered in the simulation. As a consequence, the activation energy for surface diffusion is determined by the highest barrier encountered along the diffusive paths, i.e., the energy barriers associated to jumps along the x axis. At temperatures below $T_{II}=174$ K, the surface diffusion is limited because only atomic jumps across the lowest-energy barrier of the $V(x,0)$ curve of Fig. 2 are thermally activated. This means that each adatom is confined along the x direction within one unit cell of the Si substrate. In the intermediate phase (1D lattice liquid) jumps along the y direction destroy the long-range order associated to the b_i periodicity. However, this disorder within the rows of atoms along the y axis has no effect on the adatom diffusion, as this process is controlled by an energy barrier in the x direction. Therefore the unbinding of dislocation pairs of type I at temperature $T_I=135$ K is not reflected on the value of the self-diffusion coefficient. At temperature T_{II} , the unbinding of type-II dislocations, whose Burger's vector has a finite component along the x axis, takes place. A change in the slope of the Arrhenius plot of the self-diffusion coefficient D_s is observed at temperatures $T > T_{II}$ as adatom jumps along the largest potential barriers of the $V(x,0)$ curve (see Fig. 2) are then

TABLE I. Preexponential factor D_0 and activation energy E_a corresponding to the surface self-diffusion constant D_s of the adatoms. The values for the one-dimensional diffusion coefficients D_x and D_y are also given. Two different diffusion regimes are found at low ($T < T_{II}$) and high temperatures ($T > T_{II}$).

| | $T < T_{II}$ | | $T > T_{II}$ | |
|-------|---------------------------------------|-----------------|---------------------------------------|-----------------|
| | D_0 (10^{-3} cm ² /s) | E_a (kJ/mol) | D_0 (10^{-3} cm ² /s) | E_a (kJ/mol) |
| D_s | 0.13 ± 0.01 | 4.44 ± 0.01 | 1.2 ± 0.4 | 7.60 ± 0.05 |
| D_x | 0.15 ± 0.01 | 5.0 ± 0.1 | 1.5 ± 0.9 | 8.3 ± 0.9 |
| D_y | 0.15 ± 0.02 | 4.2 ± 0.1 | 1.2 ± 0.2 | 7.2 ± 0.3 |

thermally activated. This feature differentiates the dynamic behavior of the adatoms in the 2D lattice liquid and in the intermediate phase.

V. CONCLUDING REMARKS

The Si(100)- 2×1 substrate is characterized by the presence of two different adsorption sites for physisorbed atoms as well as by pronounced anisotropy. The melting of a Xe adlayer over this substrate at coverage $\Theta = 0.85$ proceeds through two Kosterlitz-Thouless transitions due to the unbinding of dislocation pairs. The anisotropy of the surface potential allows us to distinguish between dislocations along the y axis (type I) and those having a finite x component (type II). Two free type-II dislocations of the appropriate orientation are equivalent to one free type-I dislocation (see Fig. 4). The dislocations along the y axis unbind first at temperature $T_I = 135$ K. One cannot form the remaining dislocations from the unbounded ones. Therefore a second transition appears at temperature $T_{II} = 174$ K as a consequence of the unbinding of type-II dislocations. The transition at temperature T_I is accompanied with the promotion of adatoms to the second adlayer. These melting characteristics differ from those encountered for isotropic substrates like graphite.

Disclinations are not found to play an important role in the adlayer melting over the Si(100)- 2×1 surface. The temperature dependence of the orientational order parameter p_6 of the adatoms reveals that the orientational degrees of freedom are strongly coupled to the translational ones. The substrate corrugation induces in the adlayer structure long-range order that remains at temperatures above T_{II} . These properties suggest that a hexatic phase with long-range orientational order and vanishing long-range translational order is probably not formed over the corrugated Si(100)- 2×1 surface.

The three phases found as a function of the temperature correspond to a 2D incommensurate solid, a 1D lattice liquid, and a 2D lattice liquid. The 2D solid is characterized by long-range order along the y axis given by a lattice parameter $b_i = 4.8$ Å. Along the x direction the 2D solid is commensurate with the substrate. The b_i periodicity along the y axis disappears above the temperature T_I as a consequence of the positional disorder induced by free type-I dislocations. The resulting phase can be described as a 1D lattice liquid. This assignment is justified by the similarity in the structure of the intermediate phase and the 2D lattice liquid along the y axis. We have calculated one-dimensional pair-distribution functions $g(y)$ for adatom rows parallel to the y axis. $g(y)$ is proportional to the probability of finding a Xe atom at a given y coordinate, provided that there is another atom in the same row at $y=0$. In Fig. 12 we

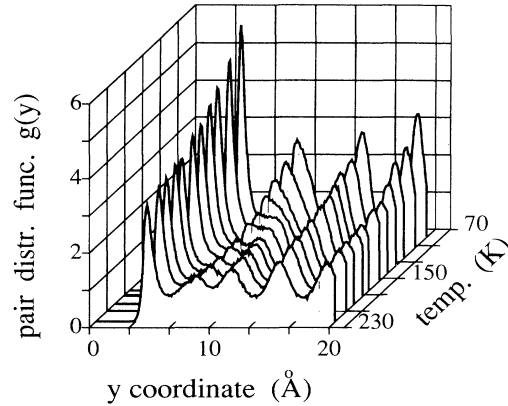


FIG. 12. One-dimensional pair-distribution function of the adatoms along the y axis as a function of the temperature. Note the splitting of the next-nearest-neighbor peak at temperatures above $T_I = 135$ K.

show the $g(y)$ curves as a function of temperature for distances up to 20 Å. The curves at the four lowest temperatures correspond to the 2D solid ($T < T_I$). The main feature of these curves is that the peak associated to the next-nearest neighbors in the 2D solid is split into two peaks at temperatures above T_I . The $g(y)$ curves corresponding to the 1D lattice liquid and the 2D lattice liquid are quite similar.

The main difference between the 1D and 2D lattice liquid arises from the dynamic properties of the adatoms. Above the temperature T_{II} the slope of the Arrhenius plot corresponding to the surface self-diffusion constant is different than below T_{II} . In the 1D lattice liquid the adatoms are confined between the highest-energy barriers of the surface potential along the x axis. However, in the 2D lattice liquid adatom jumps through those barriers are thermally activated. The intermediate phase, where the adatoms are confined between potential barriers along one direction, resembles the case of fluids confined between solid walls.²⁶ The 1D lattice liquid is characterized by pronounced disorder along one preferential direction. This anisotropy is induced by the substrate and therefore such a phase has not been described for more isotropic substrates like graphite.

ACKNOWLEDGMENTS

We thank F. Batallán and C. P. Herrero for critically reading the manuscript. The continuous interest of J. M. Serratos is also gratefully acknowledged. This work was supported by CICYT (Spain) under Contract Nos. MAT90-725 and MAT91-394.

¹K. J. Strandburg, Rev. Mod. Phys. **60**, 161 (1988).

²F. F. Abraham, Phys. Rep. **80**, 339 (1981).

³J. M. Kosterlitz and D. J. Thouless, J. Phys. C **6**, 1181 (1973).

⁴D. R. Nelson and B. I. Halperin, Phys. Rev. B **18**, 2318 (1978).

⁵A. P. Young, Phys. Rev. B **19**, 1855 (1979).

⁶N. J. Colella and R. M. Sutter, Phys. Rev. B **34**, 2052 (1986).

⁷E. D. Sprecht, M. Sutton, R. J. Birgeneau, D. E. Moncton, and P. M. Horn, Phys. Rev. B **30**, 1589 (1984).

⁸H. K. Kim, Q. M. Zhang, and M. H. W. Chan, Phys. Rev. Lett. **56**, 1579 (1986).

- ⁹Ch. Simon, I. Rosenman, F. Batallan, C. Lartigue, and J. F. Legrand, *Phys. Rev. B* **45**, 2694 (1992).
- ¹⁰P. A. Heiney, P. W. Stephens, R. J. Birgeneau, P. M. Horn, and D. E. Moncton, *Phys. Rev. B* **28**, 6416 (1983).
- ¹¹G. B. Huff and J. G. Dash, *J. Low. Temp. Phys.* **24**, 155 (1976).
- ¹²H. K. Kim and M. H. W. Chan, *Phys. Rev. Lett.* **53**, 170 (1984).
- ¹³J. Stoltenberg and O. E. Vilches, *Phys. Rev. B* **22**, 2920 (1980).
- ¹⁴E. Vives and P. Lindgård, *Phys. Rev. B* **44**, 1318 (1991).
- ¹⁵M. A. Moller and M. L. Klein, *Chem. Phys.* **129**, 235 (1989).
- ¹⁶D. Haneman, *Rep. Prog. Phys.* **50**, 1045 (1987).
- ¹⁷E. Artacho and F. Yndurain, *Phys. Rev. Lett.* **62**, 2491 (1989).
- ¹⁸C. P. Tohn and C. K. Ong, *Phys. Rev. B* **45**, 11 120 (1992).
- ¹⁹R. Ramírez, *Phys. Rev. B* **40**, 3962 (1989).
- ²⁰R. Ramírez, *Surf. Sci. Lett.* **271**, L373 (1992).
- ²¹L. Utrera and R. Ramírez, *J. Chem. Phys.* **96**, 7838 (1992).
- ²²B. W. Holland, C. B. Duke, and A. Paton, *Surf. Sci.* **140**, L249 (1984).
- ²³E. Conrad and M. B. Webb, *Surf. Sci.* **129**, 37 (1983).
- ²⁴E. G. Michel, P. Pervan, G. R. Castro, R. Miranda, and K. Wandelt, *Phys. Rev. B* **45**, 11 811 (1992).
- ²⁵G. Reiter and C. Moss, *Phys. Rev. B* **33**, 7209 (1986).
- ²⁶P. A. Thomson, G. S. Grest, and M. O. Robbins, *Phys. Rev. Lett.* **68**, 3448 (1992).